Impact of Indian Ocean Sea Surface Temperature on Developing El Niño*

H. ANNAMALAI, S. P. XIE, AND J. P. MCCREARY

International Pacific Research Center, University of Hawaii, Honolulu, Hawaii

R. MURTUGUDDE

ESSIC, University of Maryland, College Park, College Park, Maryland

(Manuscript received 12 March 2004, in final form 22 July 2004)

ABSTRACT

Prior to the 1976–77 climate shift (1950–76), sea surface temperature (SST) anomalies in the tropical Indian Ocean consisted of a basinwide warming during boreal fall of the developing phase of most El Niños, whereas after the shift (1977–99) they had an east–west asymmetry—a consequence of El Niño being associated with the Indian Ocean Dipole/Zonal mode. In this study, the possible impact of these contrasting SST patterns on the ongoing El Niño is investigated, using atmospheric reanalysis products and solutions to both an atmospheric general circulation model (AGCM) and a simple atmospheric model (LBM), with the latter used to identify basic processes. Specifically, analyses of reanalysis products during the El Niño onset indicate that after the climate shift a low-level anticyclone over the South China Sea was shifted into the Bay of Bengal and that equatorial westerly anomalies in the Pacific Ocean were considerably stronger. The present study focuses on determining influence of Indian Ocean SST on these changes.

A suite of AGCM experiments, each consisting of a 10-member ensemble, is carried out to assess the relative importance of remote (Pacific) versus local (Indian Ocean) SST anomalies in determining precipitation anomalies over the equatorial Indian Ocean. Solutions indicate that both local and remote SST anomalies are necessary for realistic simulations, with convection in the tropical west Pacific and the subsequent development of the South China Sea anticyclone being particularly sensitive to Indian Ocean SST anomalies. Prior to the climate shift, the basinwide Indian Ocean SST anomalies generate an atmospheric Kelvin wave associated with easterly flow over the equatorial west-central Pacific, thereby weakening the westerly anomalies associated with the developing El Niño. In contrast, after the shift, the east–west contrast in Indian Ocean SST anomalies does not generate a significant Kelvin wave response, and there is little effect on the El Niño–induced westerlies. The Linear Baroclinic Model (LBM) solutions confirm the AGCM's results.

1. Introduction

It is now well recognized that the El Niño–Southern Oscillation (ENSO) phenomenon is the dominant mode of tropical climate variability. Moreover, the changes in tropical precipitation and associated latent-heat release during ENSO affect the atmospheric circulation globally, primarily through wave dynamics (Hoskins and Karoly 1981; Shukla and Wallace 1983; Sardeshmukh and Hoskins 1985; Trenberth et al. 1998; Su et al. 2001). In comparison to the large fluctuations in sea surface temperature (SST) in the equatorial Pacific during ENSO, interannual SST anomalies in the Indian Ocean are modest. As a consequence, understanding their effect on the atmosphere has received less attention.

Recently, interest in the influence of Indian Ocean SSTs has expanded considerably, in part due to the debate about the Indian Ocean "Dipole/Zonal" mode (IODZM), a mode of climate variability associated with cooling in the eastern equatorial Indian Ocean during fall and warming in the western basin several months later (Reverdin et al. 1986; Murtugudde et al. 1998; Saji et al. 1999; Webster et al. 1999; Murtugudde and Busalacchi 1999; Behera et al. 1999; Yu and Rienecker 1999, 2000). The high simultaneous correlation between IODZM and Niño-3.4 SST anomalies occurs during fall, suggesting that IODZM events are forced by ENSO (e.g., Allan et al. 2001; Baquero-Bernal et al. 2002; Xie et al. 2002; Hastenrath 2002; Krishnamurthy and Kirtman 2003; Annamalai et al. 2003). Others argue that the extreme events of 1961, 1994, and 1997 are

* International Pacific Research Center Contribution Number 293 and School of Ocean and Earth Science and Technology Contribution Number 6364.

Corresponding author address: Dr. H. Annamalai, IPRC/SOEST, University of Hawaii, 1680 East West Rd., Honolulu, HI 96822.
E-mail: hanna@hawaii.edu

a coupled ocean–atmosphere mode internal to the Indian Ocean itself (e.g., Yamagata et al. 2003). As discussed below, a likely reason for the differing views is that the relationship between El Niño and IODZM events has changed in time.

Many characteristics of El Niño changed after the 1976–77 climate shift (Nitta and Yamada 1989), including its frequency, intensity, and propagation direction (Wang 1995; Wallace et al. 1998; Kinter et al. 2002, 2004). Figure 1 shows two well-known measures of ENSO: the multivariate ENSO index (Fig. 1a; Wolter and Timlin 1998) and SST anomalies over the Niño-3.4 region (Fig. 1b). Except for a few minor exceptions, both indices clearly indicate that El Niño events after the climate shift in 1976–77 were stronger than those that occurred before. Additionally, since the 1980s the ENSO period appears to have increased to 5 yr. Fedorov and Philander (2001) examined the SST anomalies over the eastern equatorial Pacific and pointed out similar changes (see Fig. 1 of their paper).

Another striking difference between the two epochs is the change in the El Niño–IODZM relationship before and after the climate shift. Figure 2 shows ENSO and IODZM indices during fall, the latter defined solely by SST anomalies in the eastern equatorial Indian Ocean (EEIO) in a box from 10°S to the equator, 90° to 110°E (Annamalai et al. 2003). Using a minimum standard deviation of ±1.0 to define ENSO and IODZM events, respectively, there were 13 El Niño (dashed lines) and 6 IODZM events during the record. An obvious difference between the PRE76 and POST76 periods is that no IODZM events cooccurred with ENSO prior to the climate shift whereas most did afterward.

In this study, we investigate the impacts of Indian Ocean SST and heating anomalies on developing El Niños, focusing on the difference in response before and after the 1976–77 climate shift. Specifically, we consider changes in their impact on the strength of the equatorial wind anomalies in the Pacific and on the formation of the South China Sea anticyclone during the fall of El Niño years (section 3). We utilize analyses of atmospheric reanalysis products, and solutions to a state-of-the-art atmospheric general circulation model (AGCM) and a linearized atmospheric model, the latter used to identify basic processes. Our main conclusions are that the presence of the IODZM modulates convective activity over the EEIO and tropical western Pacific during the developing phase of El Niño, locally altering the development of the South China Sea anticyclone, and remotely strengthening westerly anomalies in the western and central Pacific via an atmospheric Kelvin wave.

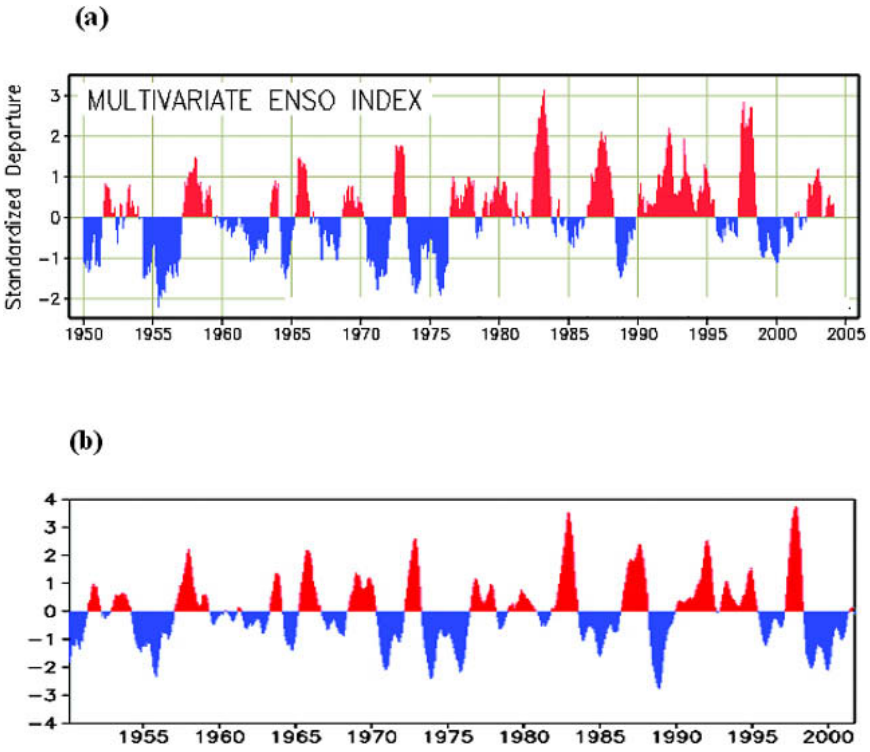

FIG. 1. (a) The multivariate ENSO index prepared by Wolter and Timlin (1998) for the period 1950–2003. (b) Monthly SST anomalies over the Niño-3.4 region (5°S–5°N, 120°–170°W). The data in (b) are smoothed by a 5-month running mean and normalized by the monthly standard deviation. Warm (cold) ENSO events are highlighted in red (blue). After the 1976–77 climate shift, the warm events are much stronger than those prior to the shift.

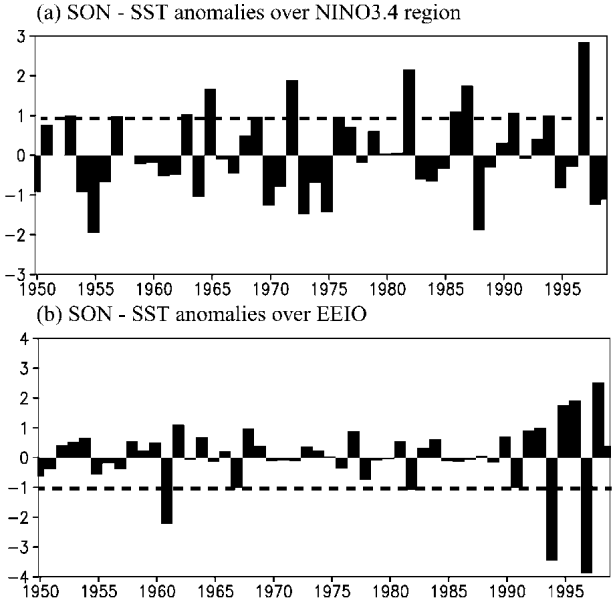

FIG. 2. Bar charts of the boreal fall (SON) SST anomalies for (a) the Niño-3.4 region (5°S–5°N, 120°–170°W) and (b) eastern equatorial Indian Ocean region (10°S–0°, 90°–110°E). The dotted horizontal lines represent −1.0 standard deviation in (b) and +1.0 standard deviation in (a). The SST anomalies are normalized with their respective standard deviations.

It should be noted that our study uses stand-alone atmospheric models to investigate changes in ENSO variability, which surely involve coupled air–sea interactions. Indeed, recent coupled modeling studies (e.g., Wu and Kirtman 2004a) suggest that experiments with prescribed SST anomalies over the Indian Ocean may distort the air–sea feedbacks between latent heat flux and SST, which lead to spurious variance in rainfall and surface wind anomalies. Our AGCM results must be viewed with this caveat in mind. On the other hand, our focus is to understand the large-scale response to Indian Ocean SST anomalies. The fact that the simulated winds over the equatorial Pacific by both the AGCM and the simple linear atmospheric model bear close resemblance to observations suggests our approach is reasonable.

The paper is organized as follows. Section 2 presents the data used and provides a brief description of the AGCM and LBM. Section 3 presents diagnostic analyses based on observations. Section 4 examines the sensitivity of the AGCM to Indo–Pacific SST anomalies. Section 5 examines the dynamical response of the LBM to diabatic heating and SST anomalies. Section 6 summarizes our conclusions.

2. Data and models

a. Data

The atmospheric data used in our study are taken from National Centers for Environmental Prediction–National Center for Atmospheric Research (NCEP–NCAR) reanalysis products for the period 1950–2001 (Kalnay et al. 1996). The atmospheric variables are available at standard pressure levels with a horizontal resolution of 2.5°. The SST for the analysis period is taken from Reynolds and Smith (1994).

In the data analyses, monthly mean climatologies are first calculated for the study period and anomalies are departures from them. Unless specified otherwise, decadal variability (periods > 8 yr) is separated from interannual variability (16 months to 8 yr) through harmonic analysis. Composites are formed for the strong El Niño years during both epochs (Fig. 2a), except that the 1986–87 event is excluded because of the complexity of its evolution with respect to the annual cycle (Wang et al. 2000) and the lack of IODZM development (Fig. 2b). Due to uncertainities in SST observations prior to the satellite era, we compared the monthly Reynolds and Smith (1994) product with the Comprehensive Ocean–Atmosphere Data Set (COADS). As in Fig. 2, we formed interannual SST anomalies over EEIO and Niño-3.4 regions (not shown) from COADS. We note high correlations (>0.7) between the corresponding indices constructed from these two datasets.

The composites (both constructed from observations and from ensembles of AGCM solutions) are subjected to the standard t test for statistical significance, and only when at the 95% significant level are retained in plots; the sole exception is for Fig. 4b, in which values significant at the 85% level are retained due to the limited members (four) in the composites. The level of significance does not alter the main conclusions of the present study that are supported by dynamical arguments (sections 4–5).

Concerning the 1986–87 event, an examination of monthly SST anomalies over the Nino-3.4 region (not shown) reveals that (i) the onset of El Niño occurred during boreal summer 1986 and attained its first peak intensity in December of that year, (ii) the amplitude of the warm SST anomalies gradually declined from 1.2°C in December 1986 to 0.7°C in June 1987, and (iii) the amplitude suddenly increased and reached its second peak (~1.7°C) in September 1987; and thereafter El Niño conditions ceased. Thus, the evolution of the 1986–87 El Niño differs markedly from other major El Niños. The Simple Ocean Data Assimilation (SODA) product, as well as solutions from ocean models, indicate that the mean thermocline was deeper than normal in the EEIO during the El Niño events of 1976 and 1986–87, conditions unfavorable for the development of the IODZM (Annamalai et al. 2004, manuscript submitted to *J. Climate*). Since our purpose is to understand the influence of the cooccurrence of IODZM events with developing El Niño in the post-1976 epoch, we excluded the 1986–87 event in our analysis. With the exclusion of the 1986–87 event, all El Niño events in the post-1976 composite are accompanied by concurrent

IOZM events while none is in the pre-1976 composite. This grouping allows us to study the effect of differing Indian Ocean SST patterns by AGCM experimentation to be described in section 4a.

Various diagnostic studies have assessed the quality of reanalyses in the Tropics, showing that the divergent part of the wind is strongly influenced by model heating, especially in data-sparse regions (e.g., Annamalai et al. 1999). For example, Kinter et al. (2004) attributed interdecadal changes in the divergent wind field in the NCEP–NCAR reanalysis to changes in the observing system and assimilation procedures [see also Wu and Xie (2003)]. Since decadal and interdecadal variability is removed in our analysis prior to making composites, effects due to changes in the observing system are minimized.

b. AGCM

The AGCM we use is the ECHAM5, the latest Hamburg version of the ECMWF model. It is a global spectral model, which we ran at T42 resolution and with 19 sigma levels in the vertical. The nonlinear terms and the parameterized physical processes are calculated on a 128×64 Gaussian grid with a horizontal resolution of about $2.8° \times 2.8°$. As in the earlier version of the model (ECHAM4, Roeckner et al. 1996), the convection scheme is based on the mass-flux concept of Tiedtke (1989); the surface fluxes of momentum, heat, water vapor, and cloud water are based on the Monin–Obukhov similarity theory, and the radiation scheme is due to Morcrette et al. (1998). Major changes to the physical package include implicit coupling of the atmosphere to the land surface (Schulz et al. 2001), advective transport (Lin and Rood 1996), a prognostic–statistical scheme for cloud cover (Tompkins 2002), and a rapid radiative-transfer model for longwave radiation (Mlawer et al. 1997). Model details can be found in Roeckner et al. (2003).

The climatology of ECHAM5 is realistic in many aspects. Figure 3 shows precipitation and 850-hPa wind during September–October–November (SON) for the model (Fig. 3a) and the observations (Fig. 3b). Model − observation differences include (i) overestimation of precipitation intensity over the tropical western Pacific and along the South Pacific convergence zone (SPCZ), (ii) a westward shift in the location of the precipitation maximum and poleward orientation of westerlies over the equatorial Indian Ocean, and (iii) cross-equatorial flow in the western Indian Ocean and penetration of westerlies into the tropical west Pacific. Despite these differences, the spatial structure and magnitude of precipitation and low-level circulation anomalies over the tropical Indo–Pacific regions are simulated reasonably well.

c. LBM

Linear atmospheric models have been widely used as a diagnostic tool for studying the response to idealized forcing (e.g., Matsuno 1966; Webster 1972; Gill 1980; Rodwell and Hoskins 1996). The linear model we use (labeled LBM) is fully described in Watanabe and Kimoto (2000) and Watanabe and Jin (2003). It is a global, time-dependent, primitive-equation model, linearized about the observed climatology derived from NCEP–NCAR reanalysis for 1958–97. Its horizontal resolution is T21 with 20 vertical levels in sigma coordinates. The model employs diffusion, Rayleigh friction, and Newtonian damping with a time scale of $(1 \text{ day})^{-1}$ for $\sigma \geq 0.9$ and $\sigma \leq 0.03$, while $(30 \text{ day})^{-1}$ is used elsewhere.

The LBM is forced either by prescribed patterns of diabatic heating anomalies or SST anomalies, referred to as dry and moist versions respectively (Watanabe and Jin 2003). In the dry version, the prescribed forcing is the anomalous diabatic heating proportional to the observed precipitation anomalies. The horizontal shape of the heating is elliptical and the heating is imposed on boreal fall (September–November) mean climatology derived from NCEP–NCAR reanalysis. The vertical heating profile is defined by an empirical function proposed by Reed and Recker (1971), with a maximum heating at 400 hPa. Since in the deep Tropics heating and circulation are strongly coupled, we also seek the steady-state response in which the LBM calculates its own heating. In this run, called moist case, the horizontal shape of the prescribed SST anomalies is assumed to be elliptical as in the dry case. The surface heat flux generated by these forcings is parameterized as in Betts and Miller (1986). A linearized moisture equation for the perturbation specific humidity is incorporated into the model. Heat and moisture sources associated with cumulus convection are also parameterized. In the moist case, mean fields of SST and ground wetness are also included in the basic state. In summary, results from the moist case can be viewed as an alternative to the AGCM solutions but within the linear framework.

3. Air–sea interaction during El Niño onset

In this section, we report the differences in SST and circulation patterns between the PRE76 and POST76 periods. Due to nonavailability of observed precipitation products over the oceans during PRE76 we have not compared the changes in the precipitation here. However, model solutions reported in section 4 illustrate the differences in the simulated precipitation to the apparent changes in SST that were used to force the AGCM.

a. SST

Figure 4 shows SST-anomaly composites from Reynolds and Smith (1994) during the fall of El Niño years before (PRE76, 1950–76) and after (POST76, 1977–99) the climate shift. During POST76 there were coherent cold SST anomalies in the EEIO and western Pacific

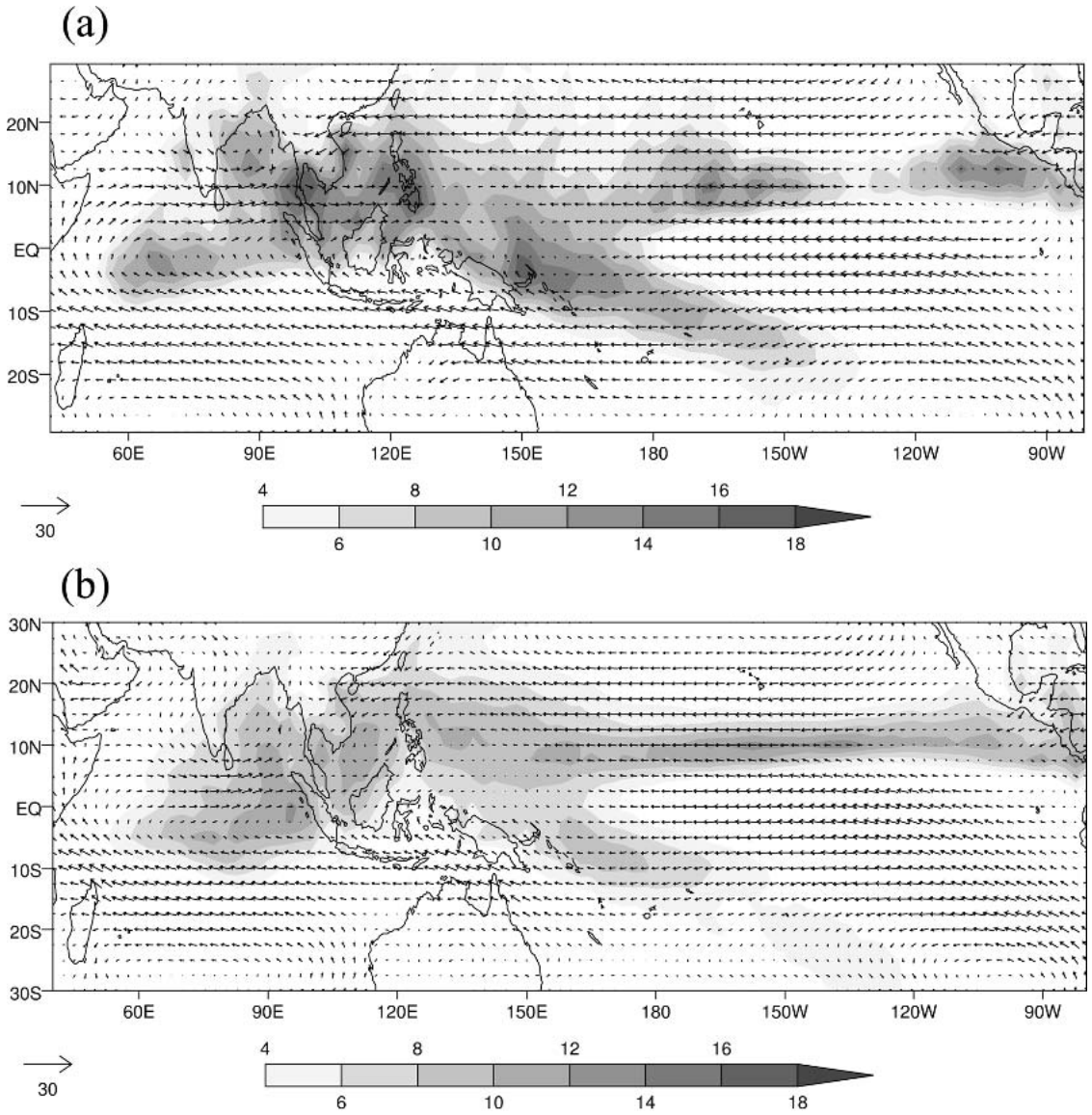

FIG. 3. (a) AGCM fall (SON) precipitation (mm day^{-1}) and 850-hPa wind (m s^{-1}) climatology from the CTL run; (b) same as (a) but from observations. The observed precipitation is from CMAP (Xie and Arkin 1996) and the wind is from NCEP–NCAR reanalysis.

that clearly stand above statistical noise (Fig. 4c). These two SST patterns occurred in conjunction with large-scale changes in winds (see below), suggesting a shift in the underlying dynamics of air–sea interaction in the region.

It is noteworthy that there is basinwide warming in the Indian Ocean during PRE76 (Fig. 4, top panel). SST observations from various sources indicate that the basinwide warming usually occurs during winter and spring *after the mature phase* of El Niño (e.g., Klein et al. 1999), and that during the preceding fall there is weak SST cooling in the EEIO, primarily due to local heat fluxes (e.g., Krishnamurthy and Kirtman 2003). The strong EEIO cooling during POST76 is a direct result of the association of ENSO and IODZM events during that epoch. Murtugudde et al. (2000) showed that the cooling resulted from ocean dynamics, with winds associated with the IODZM driving anomalous equatorial and coastal upwelling and the cool upwelled waters subsequently being advected offshore.

b. Winds

In both epochs, low-level wind anomalies have a large-scale structure, as shown by the streamfunction fields in Fig. 5. Twin anticyclones develop on either side of the equator in the Indian Ocean and South China Sea, and there are strengthened equatorial westerlies in the Pacific. During POST76, the Pacific westerlies are

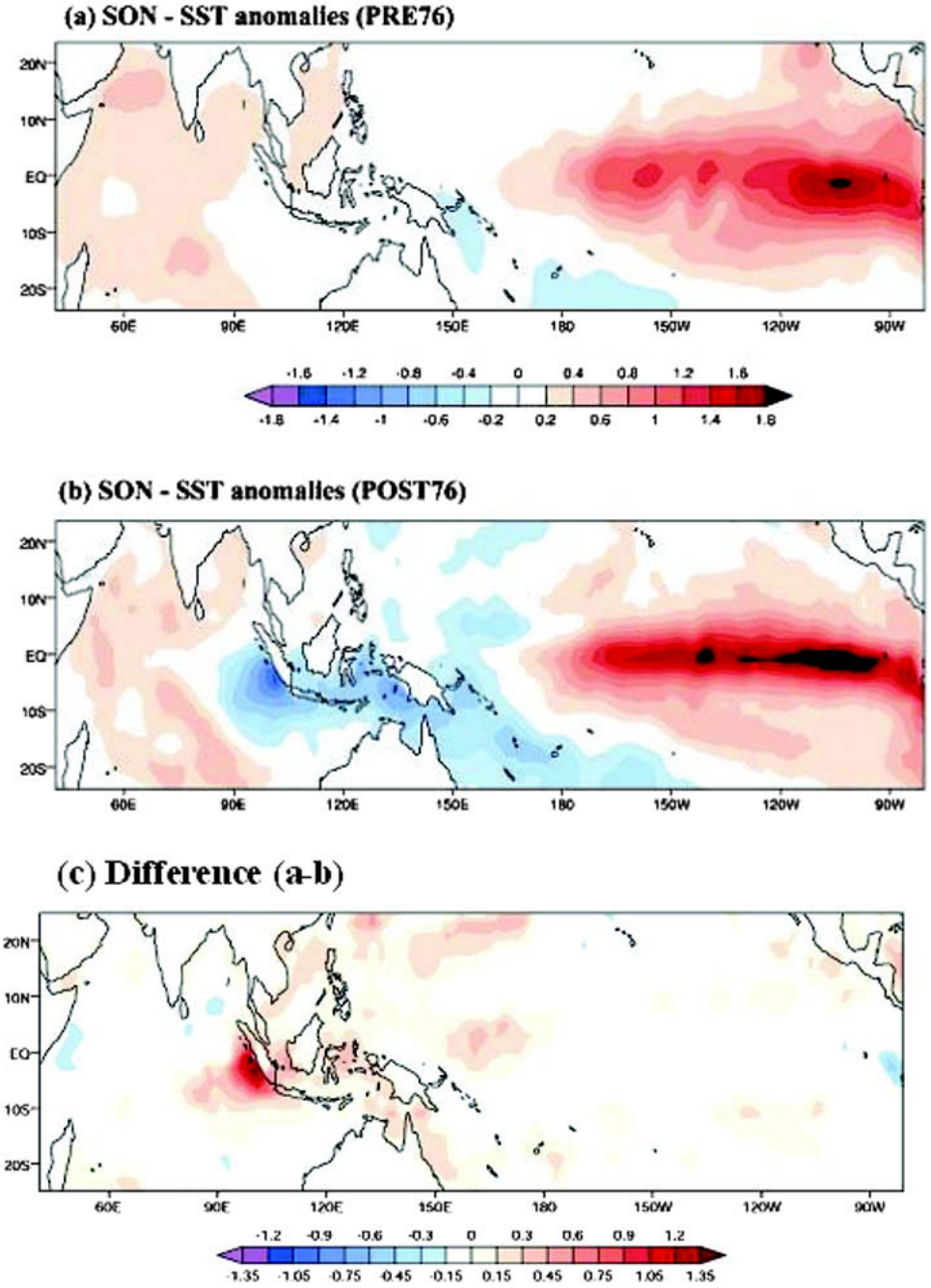

FIG. 4. Boreal fall composites of SST anomalies (°C) during El Niño years: (a) PRE76 and (b) POST76, and (c) their difference [(a) − (b)]. PRE76 (POST76) corresponds to the period 1950–75 (1977–99). The El Niño events selected during PRE76 are 1953, 1957, 1963, 1965, 1969, 1972, and 1976, and those during POST76 are 1982, 1991, 1994, and 1997. The shading interval is 0.2°C for the top two panels and 0.15°C for the bottom panel.

stronger, the northern anticyclone is weaker and shifted from the South China Sea into the Bay of Bengal, and the southern anticyclone is strengthened over the south Indian Ocean. Composite maps of 850-hPa wind anomalies (not shown) are consistent with the stream-function fields.

It is noteworthy that during POST76 the South China Sea anticyclone is not well developed (Fig. 5b), despite the higher intensity of SST anomalies over the Niño-3.4 region, and the stronger atmospheric response over the equatorial Pacific including the substantial local negative precipitation anomalies (Fig. 6b). To substantiate

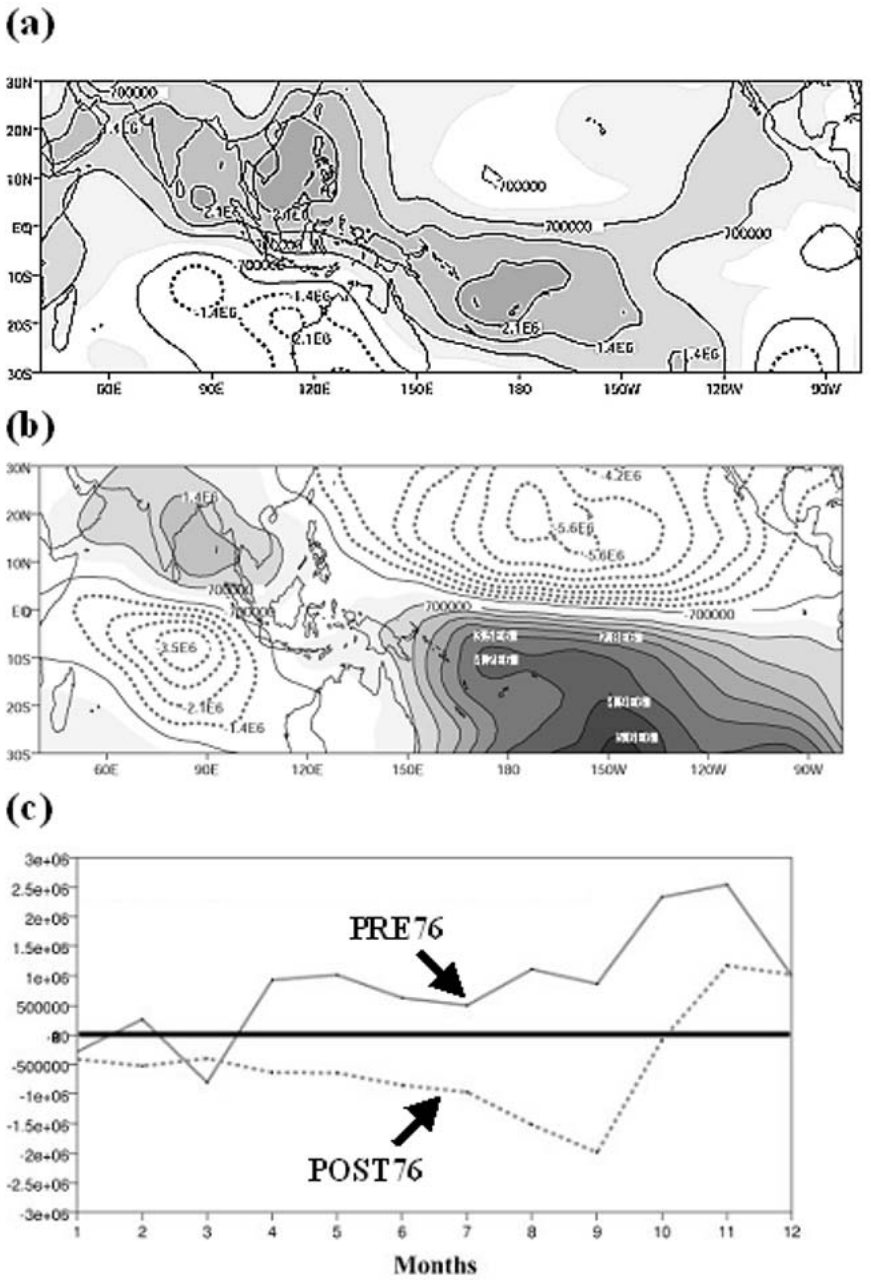

FIG. 5. Boreal fall composites of 850-hPa streamfunction anomalies for (a) PRE76 and (b) POST76, and (c) monthly composite evolution of 850-hPa streamfunction anomalies averaged over (0°–20°N, 100°–130°E), for PRE76 (solid) and POST76 (dashed). The units are $m^2\ s^{-1}$.

this result, Fig. 5c shows the monthly composite time series of 850-hPa streamfunction anomalies averaged over the tropical west Pacific. During PRE76 (solid line) a weak anticyclonic signature persists from April onward and rapidly intensifies in October. In contrast, during POST76 (dashed line) a weak cyclonic signal persists from the beginning of the year, peaking in September. Thereafter, its sign reverses but the resulting anticyclone is much weaker than its counterpart during PRE76.

Several prior studies have noted the climatic importance of the South China Sea anticyclone. Harrison and Larking (1996) first reported its presence in the western Philippine Sea during the winter of El Niño years. Wang et al. (2000) showed that it initially develops in the South China Sea, and that it subsequently modulates the East Asian monsoon, leading to stronger southerlies and enhanced precipitation over Southeast Asia. Wang et al. (2000) used both simple and comprehensive AGCMs to demonstrate that the anticyclone

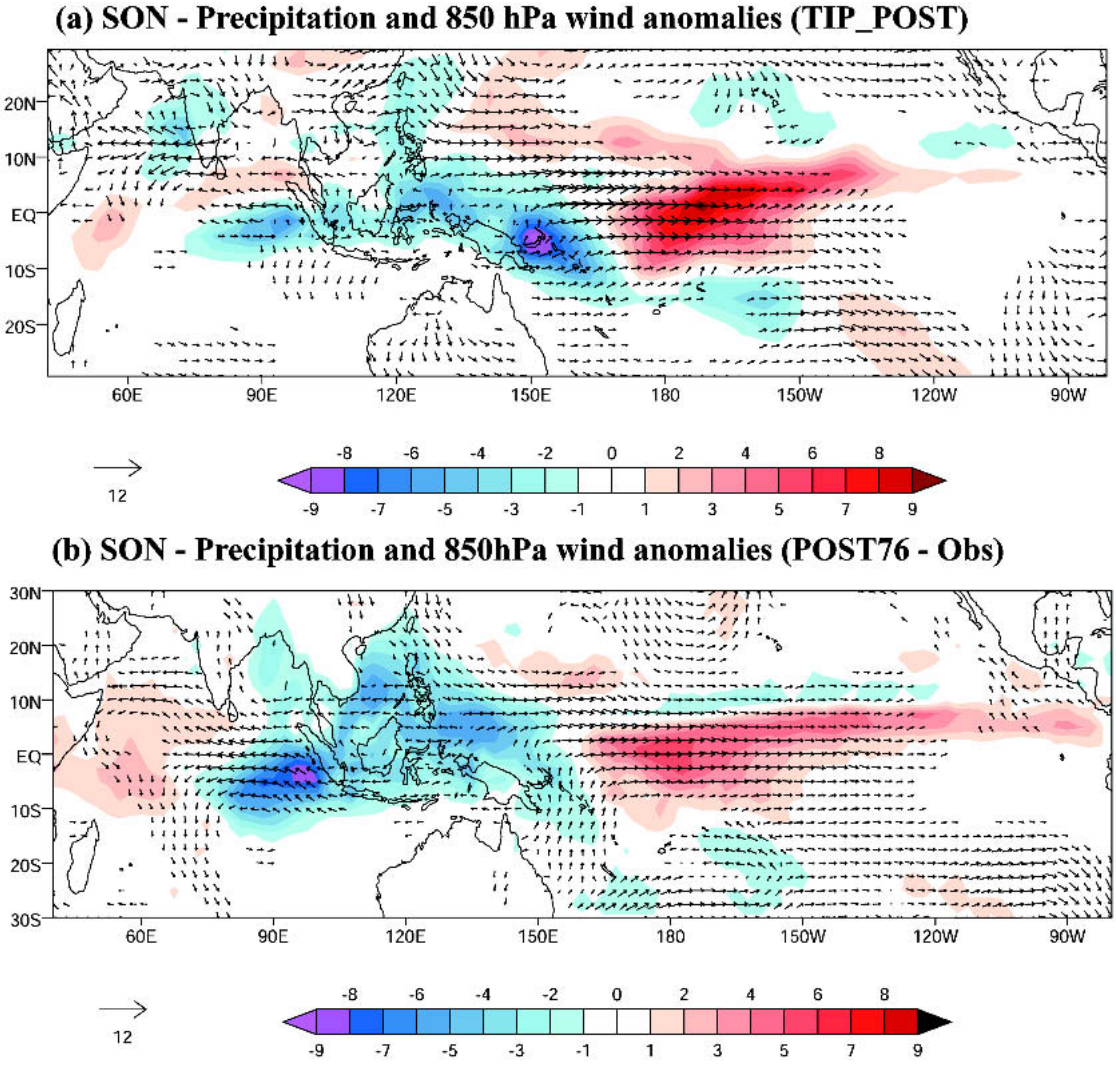

FIG. 6. (a) Anomalous precipitation (mm day^{-1}, shaded) and 850-hPa wind anomalies from the TIP_POST solutions; (b) same as (a) but from observations.

forms as a Rossby wave response to anomalous diabatic cooling associated with the weakened convection over the Maritime Continent, and Watanabe and Jin (2003) used the LBM (section 2) to arrive at the same conclusion. While Wang et al. (2000) suggested that the weakened convection is primarily associated with the eastward shift of climatological convection over the Pacific during El Niño, Watanabe and Jin (2003) emphasized that the basinwide warm SST anomalies in the Indian Ocean also contribute, acting to strengthen local convection, weaken the ascending branch of the Indian Ocean Walker circulation, and hence, decrease convection over the Maritime Continent. In a simple tropical model, Su et al. (2001) noted similar effects during the winter of the 1997–98 El Niño. In contrast, Lau and Nath (2000) concluded that the Philippine Sea anticyclone in their AGCM solutions was sensitive to Pacific SST anomalies alone. We show next that the spatial distribution of SST anomalies in the tropical Indian Ocean during fall exert considerable influence on the formation of the South China Sea anticyclone noted in Fig. 5.

4. Solutions to the AGCM

In this section, we report a suite of AGCM experiments designed to assess the influence of Indian and Pacific Ocean SST anomalies on a developing El Niño during the PRE76 and POST76 epochs. The experimental design is first discussed (section 4a), then the model's ability in simulating the basic response to Indo–Pacific SST anomalies is discussed (section 4b), and then the effect of Indian Ocean (section 4c) SST anomalies on the Pacific is presented.

a. Experimental design

Six AGCM experiments are carried out, divided into three groups. In the tropical Indo–Pacific (TIP) runs, seasonally varying SST anomalies associated with El Niño are imposed in the tropical Indo–Pacific region from 30°S to 30°N during both PRE76 and POST76 epochs (as shown for SON in Fig. 4), and seasonally varying climatological SSTs are imposed elsewhere. We refer to the two sets as TIP_PRE and TIP_POST runs, respectively. The tropical Pacific Ocean (TPO_PRE and TPO_POST) runs are similar to the two TIP runs, except that SST anomalies are inserted only in the tropical Pacific. Similarly, the tropical Indian Ocean (TIO_PRE and TIO_POST) runs are like the TIP runs, but SST anomalies are imposed only in the tropical Indian Ocean. These sets of experiments are expected to reveal the individual and combined effects of SST anomalies on the local and remote climate variability. For instance, the difference between TIP and TPO solutions will suggest the effect of Indian Ocean SST anomalies when the Pacific SST effect is interactive while that of the TIO and TPO solutions will indicate the exclusive and noninteractive effect of the individual oceans. The primary motivation for conducting these experiments is as follows: the SST anomalies over the tropical Indian Ocean often cooccur with those in the tropical Pacific and therefore it is difficult, if not impossible, to quantify their effects separately from observations alone, and experiments with an AGCM forced with SST anomalies in each ocean basin offer a means to study their separate effects.

For each of the six forcing scenarios, the model is run for the 2 yr covering the life cycle of El Niño events, that is, from 1 January of year(0) to 31 December of year(1). To account for the atmospheric sensitivity to initial conditions, a 10-member ensemble approach, with changes only in the initial conditions selected from 10 snapshots of the climatological control run but preserving the same SST forcing, is conducted for each forcing scenario. Initial conditions are taken from the control (CTL) run in which the seasonally varying climatological SST was used as the boundary forcing. Table 1 provides some details of the experiments. Since the IODZM over the equatorial Indian Ocean peaks during boreal fall season (e.g., Saji et al. 1999), the model results are only presented for fall season of year (0), that is, during the developing phase of El Niño. In a companion study, Annamalai and Liu (2004, manuscript submitted to *Quart. J. Roy. Meteor. Soc.,* hereafter ALQJR) examine the model response during boreal summer to understand the response of the summer monsoon due to the changes in ENSO properties during POST76.

TABLE 1. A list of the AGCM experiments discussed in the text.

Expt	Forcing
CTL	Climatological but seasonally varying SST
TIP_PRE	PRE76 El Niño SST anomalies over the tropical Indo–Pacific (40ºE–80ºW) regions
TIP_POST	Same as TIP_PRE but for POST76
TPO_PRE	PRE76 El Niño SST anomalies over the tropical Pacific only (120ºE–80ºW)
TPO_POST	Same as TPO_PRE but for POST76
TIO_PRE	PRE76 El Niño SST anomalies only over the tropical Indian Ocean (40º–120ºE)
TIP_POST	Same as TIO_PRE but for POST76

b. Basic response to Indo–Pacific SST anomalies

For brevity, we have not shown all of the individual TIP and TPO solutions. To assess the AGCM's fidelity in simulating the basic response, as an example, we show the TIP_POST solutions (Fig. 6a) and compare them with observations (Fig. 6b). Both in model solutions and observations, during POST76, a band of enhanced precipitation eastward of 170°E occupies the equatorial Pacific while reduced precipitation covers the tropical west Pacific, extending into the Maritime Continent. The east–west dipole pattern in precipitation over the equatorial Pacific is a well-known feature during El Niño years (e.g., Lau and Nath 2000). It is rather interesting to note that negative precipitation anomalies over the EEIO (~60%–70% reduction of its climatological value) are flanked by positive anomalies in the western Indian Ocean (Figs. 6a,b). This east–west contrast in precipitation anomalies over the equatorial Indian Ocean is associated with corresponding changes in the SST distribution (Fig. 4b). While westerly wind anomalies dominate the equatorial Pacific, easterly wind anomalies prevail over the equatorial Indian Ocean. In summary, the salient features of the individual TIP and TPO solutions include (i) all four solutions have similar spatial distribution of precipitation and wind anomalies over the Pacific demonstrating the dominant influence of Pacific SST anomalies in determining the atmospheric response there and (ii) the solutions obtained by the TIP_POST and TPO_POST runs indicate that about 20%–25% of the EEIO precipitation variability is forced by Pacific SST anomalies alone. The close similarity between the model solutions and observations (e.g., Fig. 6) paves the way for isolating and understanding the possible effect of Indian Ocean SST anomalies on the Pacific climate.

c. Influence of Indian Ocean SST anomalies

First, we show the TIP − TPO difference plot (Fig. 7), which will shed light on the local and remote impact of Indian Ocean SST anomalies that can be directly compared with TIO solutions (Fig. 8). The difference between the TIP_PRE and TPO_PRE runs (Fig. 7a) indicates substantial anomalies of precipitation not only in the Indian Ocean but in the tropical West Pacific as well. During PRE76, basinwide positive precipitation anomalies over the Indian Ocean are accompanied by a significant reduction in precipitation and anticyclonic

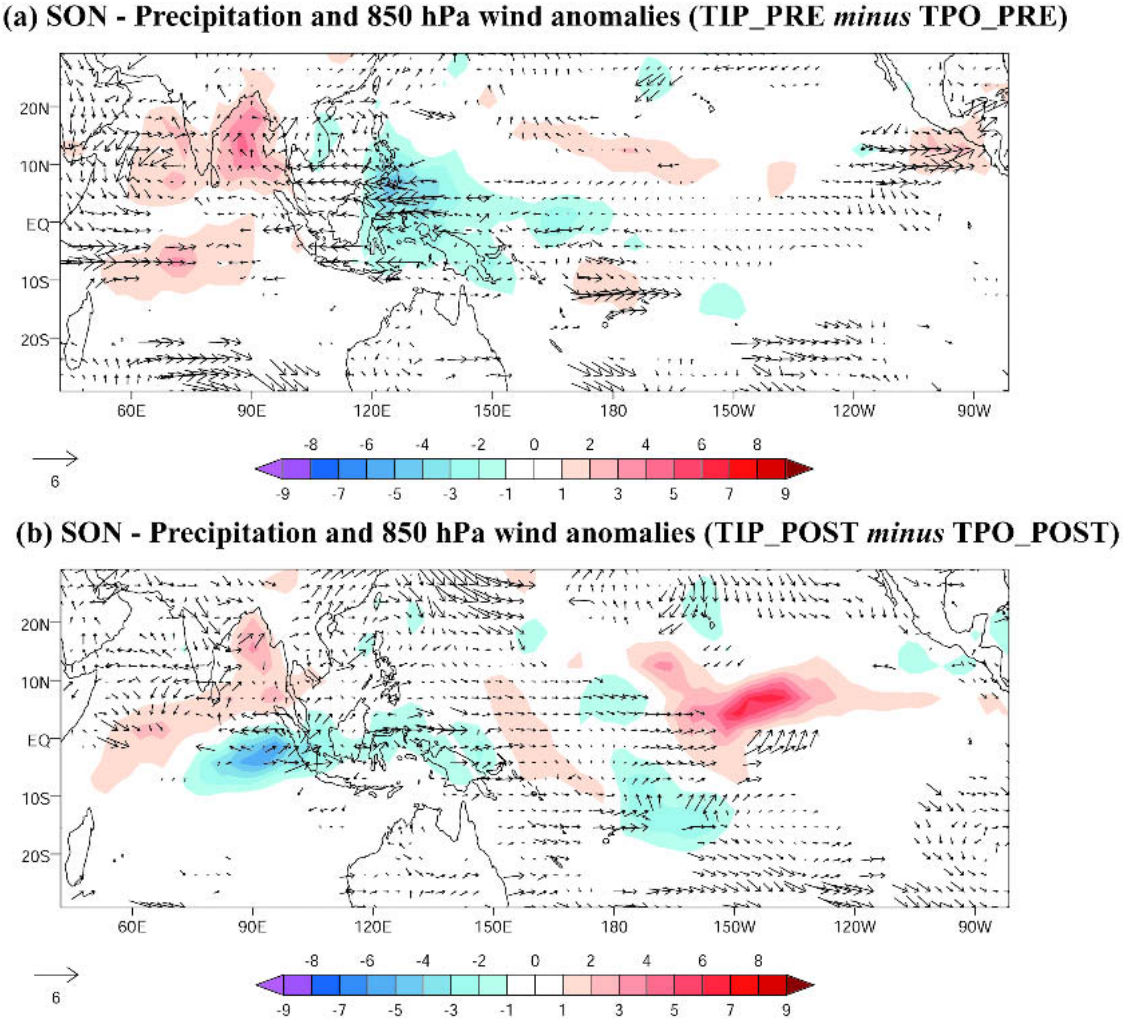

FIG. 7. AGCM-simulated precipitation difference (mm day^{-1}) in color shading and 850-hPa wind (m s^{-1}) difference between the TIP and TPO solutions during fall. This figure highlights the role of Indian Ocean SST anomalies in local and remote variations in precipitation and 850-hPa winds.

circulation anomalies over the tropical west Pacific (Fig. 7a). In contrast, during POST76 an east–west gradient in precipitation along the equatorial Indian Ocean is accompanied by near-normal precipitation over the tropical west Pacific (Fig. 7b). Therefore, this change in precipitation response in the tropical west Pacific and the lack of the South China Sea anticyclone during POST76 (Fig. 7b) attest to changes in the heating distributions in the equatorial Indian Ocean.

To isolate the effect of Indian Ocean SST on the Pacific, additional experiments forced with only the Indian Ocean SST anomalies are carried out. An additional advantage of the TIO runs is that they aid in assessing the nonlinearity by comparing with the TIP − TPO difference maps (e.g., Fig. 7). The large-scale response, however, appears to be linear in that anomalies are similar in Figs. 7 and 8 except for the positive precipitation anomalies over the equatorial central Pacific and associated westerly wind anomalies during POST76 (Fig. 7b). Thus, the inclusion of Indian Ocean SST anomalies together with those over the tropical Pacific results in an increase in precipitation over the equatorial Pacific possibly due to nonlinear and interactive effects.

In TIO_PRE, as a direct response to basinwide warm SST anomalies, precipitation increases over the tropical Indian Ocean (Fig. 8a) and easterly (westerly) wind anomalies dominate the eastern (western) Indian Ocean but slightly north (south) of the equator. Consistent with observations (section 3), in the AGCM solutions that include the effect of Indian Ocean SST anomalies, the most conspicuous feature in the TIO_PRE run is the suppression of precipitation over the tropical west Pacific and its enhancement in the Indian Ocean. The precipitation response in the TIO_POST run differs considerably from that in TIO_PRE. In the

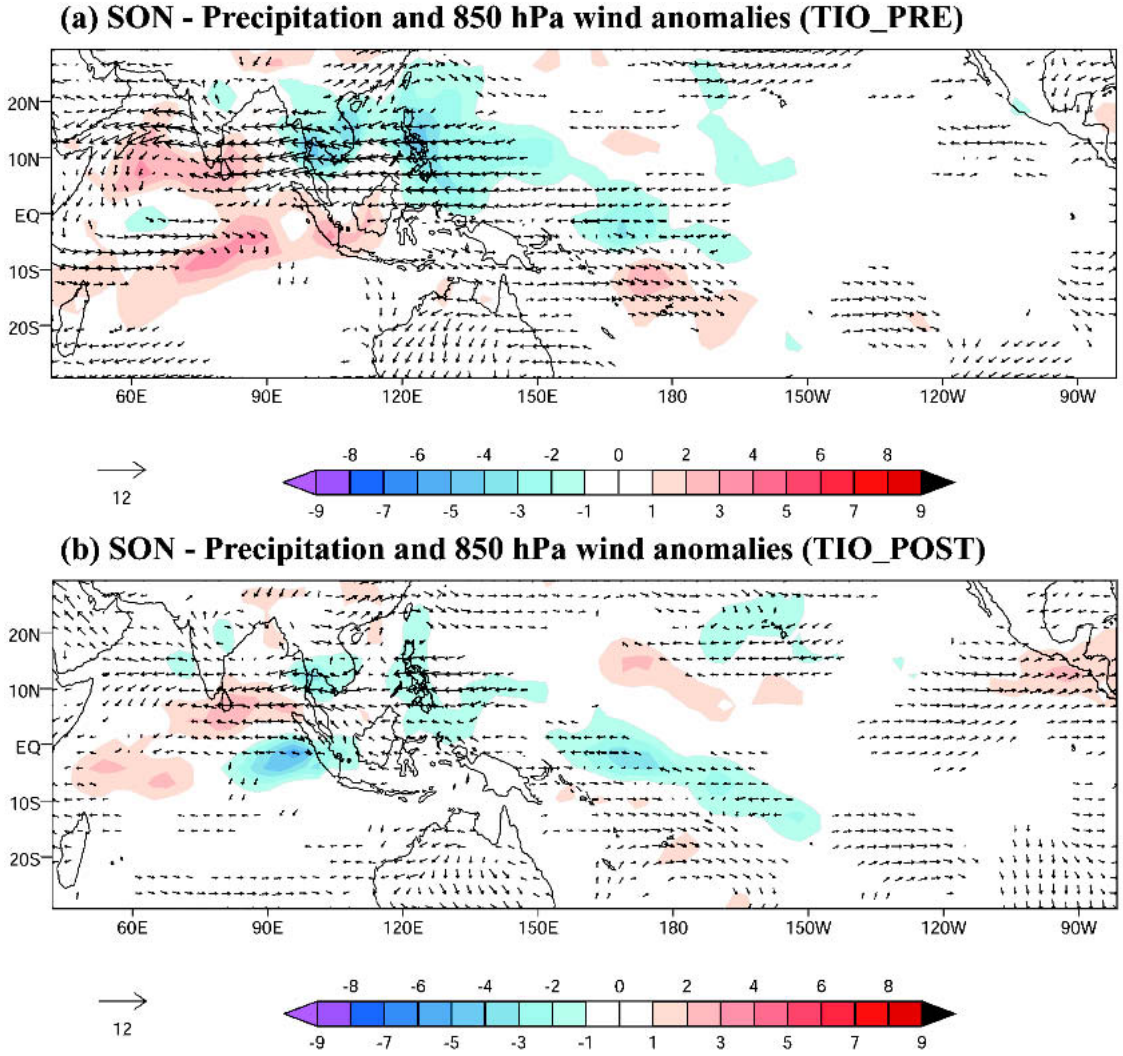

FIG. 8. Precipitation (mm day^{-1}) and 850-hPa wind (m s^{-1}) anomalies obtained from the AGCM solutions (a) TIO_PRE and (b) TIO_POST. The anomalies refer to ensemble mean minus the model climatology. The precipitation values are shaded in colors while the reference wind vector is also shown. Table 1 and section 4a explain the acronyms.

TIO_POST run (Fig. 8b) there are negative precipitation anomalies in the EEIO with positive precipitation anomalies located to the north and west of it. In response to the east–west contrast in precipitation, there are easterly wind anomalies along the equatorial Indian Ocean. Unlike the TIO_PRE run the precipitation response outside the basin, particularly over the tropical west Pacific, is marginal. These results confirm the sensitivity of tropical west Pacific convection to the *spatial distribution* of Indian Ocean SST anomalies. It is interesting to note that in both epochs (Fig. 8) positive precipitation anomalies over Sri Lanka are largely due to in situ warm SST anomalies (Fig. 4).

We now turn our focus to the effect of Indian Ocean SST anomalies on the equatorial Pacific wind. In the TIO_PRE run, easterly wind anomalies are excited along the equatorial west-central Pacific as a Kelvin wave response to anomalous Indian Ocean precipitation. In contrast, in TIO_POST, despite a realistic simulation of negative precipitation anomalies over the EEIO that in isolation by themselves would induce anomalous westerlies to the east, westerly wind anomalies in the west-central Pacific are not apparent. Instead, weak easterly wind anomalies are noted there. One possible explanation is that the anomalous precipitation patterns (positive in the west and negative in the east) lie within the equatorial Rossby radius, and hence the Kelvin wave response to both positive and negative convective anomalies in the Indian Ocean cancels each other out.

One caveat in the TIO_PRE solutions is the dominance of easterly wind anomalies between 10°N and 0° over the eastern Indian Ocean and westerly wind anomalies over 10°S to 0° in the western Indian Ocean.

Examination of a composite of observed winds at 850 hPa for PRE76 (Fig. 5a) reveals the dominance of easterly wind anomalies over the equatorial Indian Ocean (10°S–10°N). This systematic error in the TIO_PRE solutions appears to be a Rossby wave response to the positive precipitation anomalies over the equatorial western central Indian Ocean. Presumably, they are related to systematic errors in the model mean precipitation climatology in the western Indian Ocean noted earlier (Fig. 3a).

5. Solutions to the LBM

An AGCM's response to imposed SST anomalies generally depends on the model's basic state (e.g., Shukla 1984; Lau and Nath 2000; Kang et al. 2002). In the AGCM used here, a deficiency of the basic state is the westward shift in the precipitation climatology over the equatorial Indian Ocean (Fig. 3a) and the associated error in the simulated wind anomalies discussed in section 4c. For this reason, here we consider solutions to the LBM, for which the background state is prescribed. The LBM solutions therefore provide an alternate, and clarifying, view of the basic dynamics.

a. Experimental design

As mentioned in section 2, solutions are obtained for both dry and moist versions of the LBM, forced by idealized diabatic heating and SST anomalies, respectively, that mimic observed precipitation patterns in the equatorial Indian Ocean.

The dry version of the LBM is forced by the column-integrated heating profiles shown in Figs. 9a and 9b. To represent the basinwide heating anomaly typical of the PRE76 period, we impose diabatic heating anomalies centered at equator, 70°E with a heating rate of about 2 K day^{-1} at 400 hPa. The zonal and meridional extent of the heating anomalies are 40° and 20°, respectively. To represent the dipolelike precipitation anomalies during POST76, we include diabatic heating and cooling anomalies centered near 5°S, 60°E and 5°S, 90°E, respectively, with heating rates of about $\pm$2 K day^{-1} at 400 hPa. The zonal and meridional extent for both the heating and cooling anomalies is 20° and 10°, respectively. For the moist LBM driven by SST anomalies, the magnitude and location of maximum anomalies are chosen based on Fig. 4, and the zonal and meridional extent of the anomalies are similar to the dry case. Figures 10a and 10b show the resulting model-generated heating patterns averaged over the entire atmospheric column. The LBM is integrated for 30 days, attains a steady state in about 10–15 days, and the response at day 20 is analyzed.

b. Dynamics

Figure 9 (Fig. 10) shows the steady-state response of the winds at 850 hPa for the dry (moist) case. In both dry and moist solutions, the response for basinwide warming and IODZM forcing scenarios depicts considerable difference over the equatorial Indo–Pacific region. Consistent with the AGCM simulations (e.g., Fig. 8b), for IODZM-related easterly wind forcing anomalies occupy the equatorial Indian Ocean. As in the observations (Fig. 5b) twin anticyclonic circulations are prominent in the eastern Indian Ocean, and the Southern Hemispheric component is stronger than its Northern Hemispheric counterpart. From linear theory, the intensity of the wave response depends on the "zonal distance" between the heat sources or sinks (e.g., Gill 1980). Since the heating anomalies during IODZM years are placed "too close" in the zonal direction in the equatorial Indian Ocean, in both dry and moist runs the magnitude of the simulated westerly wind anomalies in the equatorial western central Pacific ($<$1 m s^{-1}) are weak due to destructive interference. As suggested in section 4c, the LBM solution confirms the cancellation effect of the Kelvin wave responses to positive and negative diabatic heating in the equatorial Indian Ocean.

For the basinwide forcing scenario in the LBM (Figs. 9c and 10c), twin cyclones on either side of the equator in the western Indian Ocean as a Rossby wave response are prominent. The Kelvin wave generates easterly wind anomalies and the associated divergence extends into the tropical west Pacific with the maximum response centered at 5°N, 140°E. In the moist case (Figs. 10a and 10c), due to the interactive nature between the circulation and heating anomalies, weak negative diabatic heating anomalies are generated over the Maritime Continent and the South China Sea (Fig. 10a), much as in the AGCM TIO-PRE run (Fig. 7a). As a result of this negative heating, the equatorial easterlies over the Pacific are weaker (Fig. 10c) than in the dry case (Fig. 9c). In both basinwide and IODZM SST anomaly runs the moist solutions capture additional heating anomalies induced by circulation changes (Figs. 10a and 10b).

c. Impacts on El Niño

The AGCM and LBM solutions suggest that during years when basinwide warming occurs in the Indian Ocean, the associated positive precipitation anomalies generate easterly wind anomalies in the equatorial western Pacific. In such circumstances, the Indian Ocean heating anomalies would weaken the ongoing El Niño. On the other hand, during IODZM years the net precipitation anomaly over the Indian Ocean is weak, exciting little net Kelvin wave response over the equatorial western Pacific and allowing the ongoing El Niño to grow. Figure 11a shows a composite evolution of observed 850-hPa wind anomalies averaged over the equatorial west-central Pacific for the PRE76 and POST76 epochs. Consistent with the model solutions, during PRE76 the westerly wind anomalies in the equatorial west Pacific show little change during August–

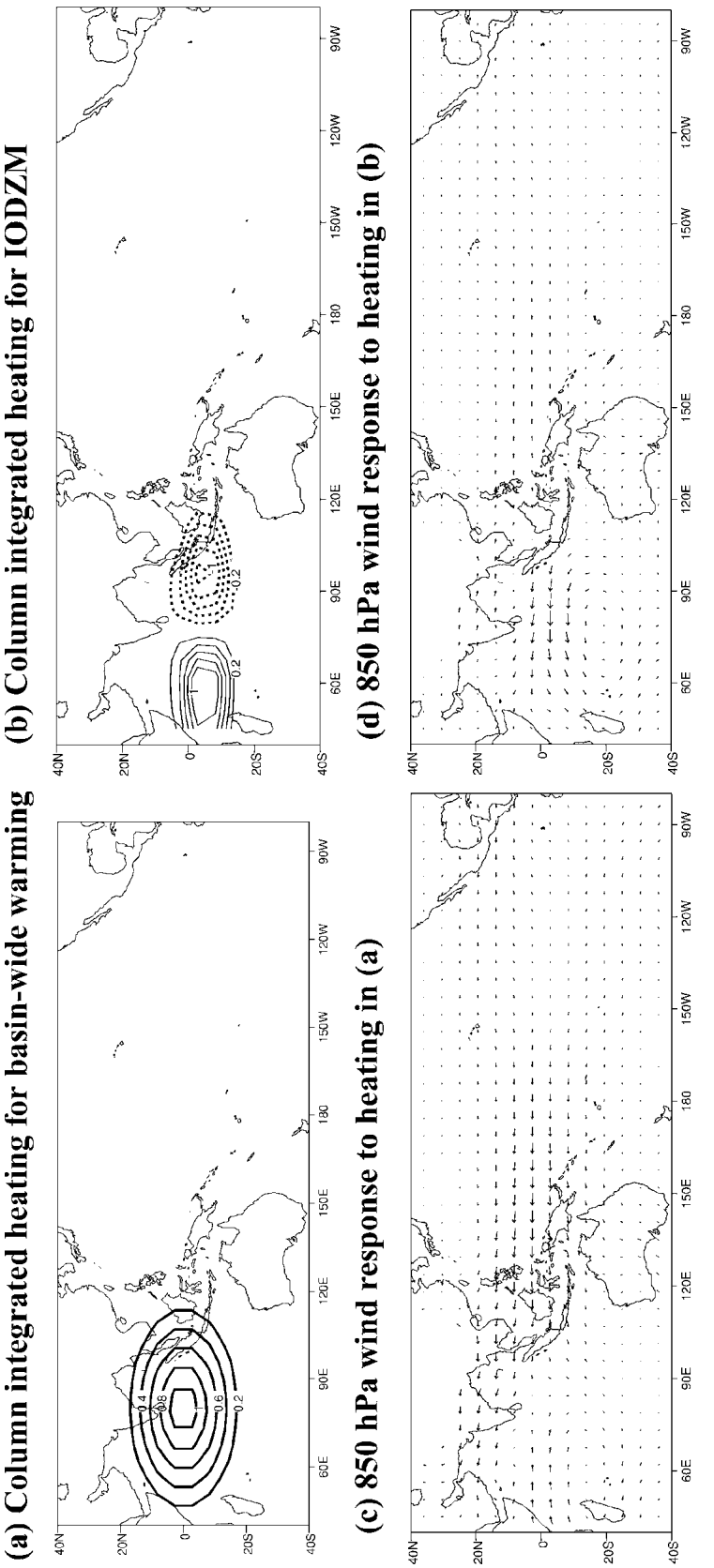

FIG. 9. (a) Vertical column–integrated diabatic heating anomalies (K day^{-1}) imposed for the basinwide warming scenario; (b) same as (a) but for IODZM heating; (c) perturbation wind response at 850 hPa for heating pattern shown in (a); and (d) same as (c) but for the heating pattern shown in (b). The LBM is run in "dry" mode. Contour interval in (a) and (b) is 0.2 K day^{-1} and the reference wind vectors for (c) and (d) are also shown.

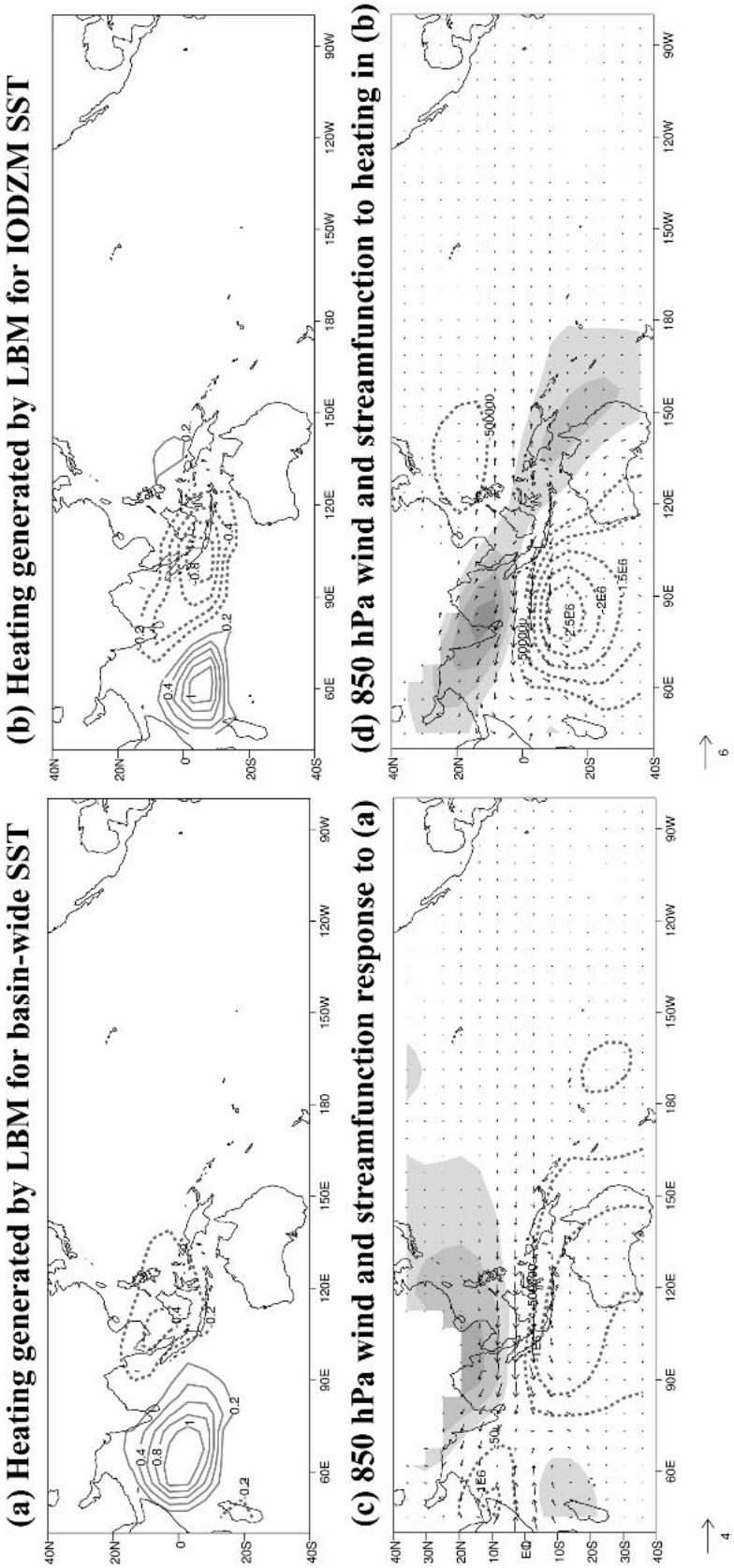

FIG. 10. As in Fig. 10 but for the moist LBM run. SST anomalies as shown in Fig. 2 are prescribed and the model-generated heating anomalies (K day^{-1}) integrated over the vertical column are shown in (a) and (b), and the corresponding 850-hPa wind (m s^{-1}) and streamfunction (10^6 m^2 s^{-1}) anomalies are shown in shading in (c) and (d), respectively. The contour intervals in (a) and (b) are 0.2 K day. The shading intervals in (c) and (d) are 0.5e+06; negative values are shown as contours while positive values are shaded.

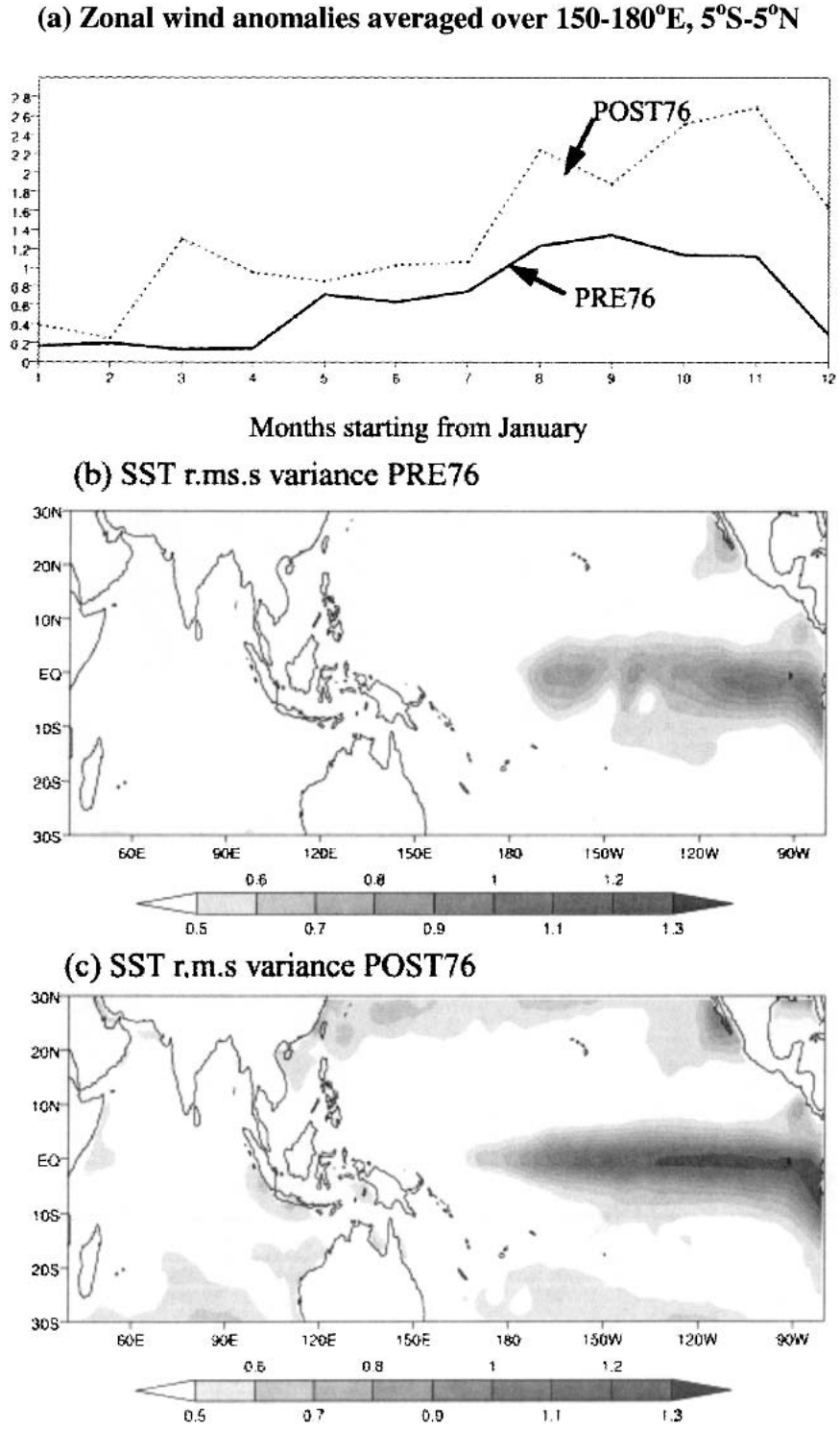

FIG. 11. (a) Composite evolution of zonal wind anomalies (m s^{-1}) averaged over the equatorial west-central Pacific during PRE76 (black line) and POST76 (red line) El Niños, root-mean-square variance of SST (°C) during Dec–Feb during (b) PRE76 and (c) POST76.

November. In sharp contrast in POST76, the anomalous westerlies amplify rapidly in July–October, a period during which the Sumatra cooling grows and reduces the Indian Ocean effect on the west Pacific. Our results from observations and AGCM and LBM solutions paint a coherent picture that Indian Ocean heating anomalies do influence the amplitude of the zonal wind anomalies in the equatorial west-central

Pacific, which in turn impact the thermocline in the eastern equatorial Pacific and affect the growth/development of El Niño in the Pacific (e.g., McCreary 1976). The 1982–83 and 1997–98 El Niños, the strongest events on record, are likely to be aided in their growth by the cooling over the EEIO. The observed SST variance at the peak phase of ENSO (December–February) clearly indicates that the POST76 ENSO events are much stronger than those in PRE76 (Figs. 11b,c).

As mentioned in the introduction previous studies have identified the changes in the strength of El Niño during POST76 (e.g., Wallace et al. 1998). Many factors influence the statistical properties of El Niño, namely (i) nonlinearity (Timmermann et al. 2003; An and Jin 2004), (ii) decadal variability in the mean state (Fedorov and Philander 2001; Wang and An 2001), (iii) stochastic forcing (Timmermann and Jin 2002), (iv) monsoon variability (e.g., Wainer and Webster 1996; Chung and Nigam 1999; Kirtman and Shukla 2000; Wu and Kirtman 2003), and (v) convective anomalies over the equatorial west Pacific (Nicholls 1984; Weisberg and Wang 1997). The strongest El Niño of the previous century occurred during 1997–98 when Pacific decadal variability was in its transition phase. During IODZM years in POST76, the July–August rainfall over the monsoon region increased despite the suppressing effect of El Niño (e.g., Annamalai et al. 2003; ALQJR). Therefore, among other factors, the dramatic changes in the spatial distribution of SST anomalies over the Indian Ocean (Fig. 4) may have also played a role in the amplification of the ongoing El Niño events. Landsea and Knaff (2000) presented the limitations of state-of-art coupled general circulation models (CGCMs) in predicting the intensity of the 1997–98 El Niño. If our hypothesis is correct, then El Niño events with cooccurring IODZM events are stronger than those without, a preposition being tested currently by the authors in CGCMs.

d. Impacts on the South China Sea anticyclone

Both AGCM and LBM solutions indicate that the basinwide warming in the Indian Ocean induces divergence over the western Pacific that reduces the precipitation there and aids in rapid development of the anticyclone over the South China Sea (Fig. 10c). In contrast, during IODZM years the net Kelvin wave response is too weak to exert any influence on west Pacific convection (Fig. 10d). This simple mechanism, possibly, explains why the anticyclone developed during PRE76 but not in POST76.

6. Summary and discussion

In the present study, we investigate teleconnections from the equatorial Indian Ocean to the Pacific. More specifically, we explore the hypothesis that atmospheric Kelvin waves, generated by convective anomalies in the equatorial Indian Ocean during fall of El Niño years, establish equatorial wind anomalies that subsequently influence the ongoing El Niño.

To identify the influence of equatorial Indian Ocean SST anomalies, we made composites of the SST and streamfunction field at 850 hPa over the tropical Indo–Pacific regions separately for PRE76 (1950–75) and POST76 (1977–99) El Niño events (section 3). In both epochs, the anomalous heating and associated circulation response in the equatorial Pacific are overall similar. Over the Indian Ocean, however, a basinwide warming (east–west gradient) prevails in SST anomalies during PRE76 (POST76). An important difference between the epochs is the formation (absence) of the South China Sea anticyclone during PRE76 (POST76). Despite the higher intensity of SST anomalies over the Niño-3.4 region during POST76, the lack of a South China Sea anticyclone is attributed to the differences in the Indian Ocean SST anomalies.

To assess the relative roles of local versus remote forcing on the convective anomalies over the Indian Ocean, a suite of atmospheric model experiments is carried out (section 4a). Using the AGCM, 10-member ensemble simulations, separately for PRE76 and POST76 El Niño events, are conducted. The AGCM results demonstrate that tropical west Pacific convection and the subsequent development of the South China Sea anticyclone are sensitive to Indian Ocean SST anomalies (section 4c). In the PRE76 case, the basinwide SST anomalies over the Indian Ocean force easterly wind anomalies over the near-equatorial western central Pacific, whereas in POST76 the east–west contrast in the SST anomalies weaken the easterly wind anomalies over the equatorial Pacific (section 4c).

During IODZM years, the positive and negative precipitation anomalies over the tropical Indian Ocean exist well within the dissipation radius of Kelvin waves, resulting in the cancellation of the Kelvin wave response to this zonal dipole of precipitation anomalies. In sharp contrast, the Kelvin wave response to basinwide heating anomalies in the Indian Ocean promotes easterly wind anomalies over the tropical west Pacific. In either case, circulation anomalies induced by Indian Ocean heating anomalies can *modulate the ongoing El Niño*. In the former (latter) case, it would strength (weaken) the ongoing El Niño.

Idealized experiments with a linear model indicate that the Kelvin wave response cancels out when both positive and negative heating anomalies coexist along the equatorial Indian Ocean. Based on the dynamical interpretations offered here, it is our opinion that the IODZM in POST76, to a certain degree, would have contributed to the intensity of the El Niños in POST76. Our results are, however, constrained by the limited number of samples during POST76, and to overcome this we are currently analyzing a long run of a coupled model.

Observational studies (Barnett 1983; Behera and

Yamagata 2003) and coupled modeling studies (e.g., Anderson and McCreary 1985; Yu et al. 2002; Wu and Kirtman 2004b) indicate that circulation anomalies forced by Indian Ocean SST anomalies can influence SST variance in the equatorial Pacific. Our results further strengthen these recent studies. Therefore, identification of the Indian Ocean effect on El Niño calls for accurate measurement of SST and surface wind over the tropical Indian Ocean and further studies on its dynamics.

Acknowledgments. This research is supported by the NOAA–OGP CLIVAR Pacific Program and by the Japan Agency for Marine–Earth Science and Technology (JAMSTEC) through its sponsorship of the International Pacific Research Center (IPRC). Additional support is provided by the K. C. Wong Education Foundation (SPX) and NOAA Grant NA03OAR4310124 (RM). The Max Planck Institute makes the ECHAM model available to the IPRC under a cooperative agreement. Dr. Watanabe is acknowledged for providing the linear model and offering valuable suggestions on its use. Dr. Niklas Schneider shared his experience with the COADS dataset. Valuable comments from the anonymous reviewers are greatly appreciated.

REFERENCES

Allan, R. J., and Coauthors, 2001: Is there an Indian Ocean dipole independent of the El Niño-Southern Oscillations? *CLIVAR Exchanges,* Vol. 6, No. 3, International CLIVAR Project Office, Southampton, United Kingdom, 18–22.

An, S. I., and F. F. Jin, 2004: Nonlinearity and asymmetry of ENSO. *J. Climate,* **17,** 2399–2412.

Anderson, D. L. T., and J. P. McCreary, 1985: On the role of the Indian Ocean in a coupled ocean–atmosphere model of El Niño and the Southern Oscillation. *J. Atmos. Sci.,* **42,** 2439–2444.

Annamalai, H., H., J. M. Slingo, K. R. Sperber, and K. Hodges, 1999: The mean evolution and variability of the Asian summer monsoon: Comparison of ECMWF and NCEP–NCAR reanalyses. *Mon. Wea. Rev.,* **127,** 1157–1186.

——, R. Murtugudde, J. Potemra, S. P. Xie, P. Liu, and B. Wang, 2003: Coupled dynamics in the Indian Ocean: Spring initiation of the zonal mode. *Deep-Sea Res.,* **50B,** 2305–2330.

Baquero-Bernal, A., M. Latif, and S. Legutke, 2002: On dipolelike variability of sea surface temperature in the tropical Indian Ocean. *J. Climate,* **15,** 1358–1368.

Barnett, T. P., 1983: Interaction of the monsoon and Pacific trade wind system at interannual time scales. Part I: The equatorial zone. *Mon. Wea. Rev.,* **111,** 756–773.

Behera, S. K., and T. Yamagata, 2003: Influence of the Indian Ocean dipole on the Southern Oscillation. *J. Meteor. Soc. Japan,* **81,** 169–177.

——, R. Krishnan, and T. Yamagata, 1999: Unusual ocean–atmosphere conditions in the tropical Indian Ocean during 1994. *Geophys. Res. Lett.,* **26,** 3001–3004.

Betts, A., and M. J. Miller, 1986: A new convective adjustment scheme. Part II: Single column tests using GATE wave, BOMEX, ATEX, and artic air-mass data sets. *Quart. J. Roy. Meteor. Soc.,* **112,** 693–709.

Chung, C., and S. Nigam, 1999: Asian summer monsoon–ENSO feedback on the Cane–Zebiak model ENSO. *J. Climate,* **12,** 2787–2807.

Fedorov, A. V., and G. H. Philander, 2001: A stability analysis of tropical ocean–atmosphere interactions: Bridging measurements and theory for El Niño. *J. Climate,* **14,** 3086–3101.

Gill, A. E., 1980: Some simple solutions for heat induced tropical circulation. *Quart. J. Roy. Meteor. Soc.,* **106,** 447–462.

Harrison, D. E., and N. K. Larking, 1996: The COADS sea level pressure signal: A near-global El Niño composite and time series view, 1946–93. *J. Climate,* **9,** 3025–3055.

Hastenrath, S., 2002: Dipoles, temperature gradients, and tropical climate anomalies. *Bull. Amer. Meteor. Soc.,* **83,** 735–740.

Hoskins, B. J., and D. J. Karoly, 1981: The steady linear response of a spherical atmosphere to thermal and orographic forcing. *J. Atmos. Sci.,* **38,** 1179–1196.

Kalnay, E., and Coauthors, 1996: NCEP/NCAR 40-Year Reanalysis Project. *Bull. Amer. Meteor. Soc.,* **77,** 437–471.

Kang, I.-S., and Coauthors, 2002: Intercomparison of GCM simulated anomalies associated with the 1997–98 El Niño. *J. Climate,* **15,** 2791–2805.

Kinter, J. L., K. Miyakoda, and S. Yang, 2002: Recent changes in the connection from the Asian monsoon to ENSO. *J. Climate,* **15,** 1203–1215.

——, M. J. Fennessy, V. Krishnamurthy, and L. Marx, 2004: An evaluation of the apparent interdecadal shift in the tropical divergent circulation in the NCEP–NCAR reanalysis. *J. Climate,* **17,** 349–361.

Kirtman, B. P., and J. Shukla, 2000: Influence of the Indian summer monsoon on ENSO. *Quart. J. Roy. Meteor. Soc.,* **126,** 1–27.

Klein, S. A., B. J. Soden, and N. C. Lau, 1999: Remote sea surface temperature variations during ENSO: Evidence for a tropical atmospheric bridge. *J. Climate,* **12,** 917–932.

Krishnamurthy, V., and B. P. Kirtman, 2003: Variability of the Indian Ocean: Relation to monsoon and ENSO. *Quart. J. Roy. Meteor. Soc.,* **129,** 1623–1646.

Landsea, C. W., and J. A. Knaff, 2000: How much skill was there in forecasting the very strong 1997–98 El Niño. *Bull. Amer. Meteor. Soc.,* **81,** 2107–2119.

Lau, N. C., and M. J. Nath, 2000: Impact of ENSO on the variability of the Asian–Australian monsoon as simulated in GCM experiments. *J. Climate,* **13,** 4287–4309.

Lin, S. J., and R. B. Rood, 1996: Multidimensional flux from Lagrangian transport. *Mon. Wea. Rev.,* **124,** 2046–2086.

Matsuno, T., 1966: Quasi-geostrophic motions in the equatorial area. *J. Meteor. Soc. Japan,* **44,** 25–43.

McCreary, J. P., 1976: Eastern tropical ocean response to changing wind systems: With application to El Niño. *J. Phys. Oceanogr.,* **6,** 632–645.

Mlawer, E. J., S. J. Taubman, P. D. Brown, M. J. Iacono, and S. A. Clough, 1997: Radiative transfer for inhomogeneous atmosphere: RRTM, a validated correlated-*k* model for the longwave. *J. Geophys. Res.,* **102,** 16 663–16 682.

Morcrette, J. J., S. A. Clough, E. J. Mlawer, and M. J. Iacono, 1998: Impact of a validated radiative transfer scheme, RRTM, on the ECMWF model climate and 10-day forecasts. ECMWF Tech. Memo. 252, Reading, United Kingdom, 47 pp.

Murtugudde, R., and A. J. Busalacchi, 1999: Interannual variability of the dynamics and thermodynamics of the tropical Indian Ocean. *J. Climate,* **12,** 2300–2326.

——, B. N. Goswami, and A. J. Busalacchi, 1998: Air–sea interaction in the southern tropical Indian Ocean and its relations to interannual variability of the monsoon over India. *Proc. Int. Conf. on Monsoon and Hydrologic Cycle,* Kyongju, Korea, Korean Meteorological Society.

—— J. P. McCreary, and A. J. Busalacchi, 2000: Oceanic processes associated with anomalous events in the Indian Ocean with relevance to 1997–98. *J. Geophys. Res.,* **105,** 3295–3306.

Nicholls, N., 1984: The Southern Oscillation and Indonesian sea surface temperature. *Mon. Wea. Rev.,* **112,** 424–432.

Nitta, T., and S. Yamada, 1989: Recent warming of tropical sea surface temperature and its relationship to the Northern Hemisphere circulation. *J. Meteor. Soc. Japan,* **67,** 375–383.

Reed, R. J., and E. E. Recker, 1971: Structure and properties of synoptic-scale wave disturbances in the equatorial western Pacific. *J. Atmos. Sci.,* **28,** 1117–1133.

Reverdin, G., D. Cadet, and D. Gutzler, 1986: Interannual displacements of convection and surface circulation over the equatorial Indian Ocean. *Quart. J. Roy. Meteor. Soc.,* **112,** 43–46.

Reynolds, R. W., and T. M. Smith, 1994: Improved global sea surface temperature analyses using optimal interpolation. *J. Climate,* **7,** 929–948.

Rodwell, M. J., and B. J. Hoskins, 1996: Monsoons and the dynamics of desert. *Quart. J. Roy. Meteor. Soc.,* **122,** 1385–1404.

Roeckner, E., and Coauthors, 1996: Atmospheric general circulation model ECHAM4: Model description and simulation of present-day climate. Max-Planck-Institut für Meteorlogie Rep. 218, Hamburg, Germany, 82 pp.

——, and Coauthors, 2003: Atmospheric general circulation model ECHAM5: Part I. Max-Planck-Institut für Meteorlogie Rep. 349, Hamburg, Germany, 140 pp.

Saji, N. H., B. N. Goswami, P. N. Vinayachandran, and T. Yamagata, 1999: A dipole mode in the tropical Indian Ocean. *Nature,* **401,** 360–363.

Sardeshmukh, P. D., and B. J. Hoskins, 1985: Vorticity balances in the tropics during the 1982–83 El Niño–Southern Oscillation event. *Quart. J. Roy. Meteor. Soc.,* **111,** 261–278.

Schulz, J. P., L. Dumenil, and J. Polcher, 2001: On the land surface atmosphere coupling and its impact in a single column atmospheric model. *J. Appl. Meteor.,* **40,** 642–663.

Shukla, J., 1984: Predictability of time averages: Part II. The influence of the boundary forcing. *Problems and Prospects in Long and Medium Range Weather Forecasting,* D. M. Burridge and E. Kallen, Eds., Springer-Verlag, 155–206.

——, and J. M. Wallace, 1983: Numerical simulation of the atmospheric response to equatorial Pacific sea surface temperature anomalies. *J. Atmos. Sci.,* **40,** 1613–1630.

Su, H., J. D. Neelin, and C. Chou, 2001: Tropical teleconnection and local response to SST anomalies during the 1997–98 El Niño. *J. Geophys. Res.,* **106,** 20 025–20 043.

Tiedtke, M., 1989: A comprehensive mass flux scheme for cumulus parameterization in a large-scale model. *Mon. Wea. Rev.,* **117,** 1779–1800.

Timmermann, A., and F. F. Jin, 2002: A nonlinear mechanism for decadal El Niño amplitude changes. *Geophys. Res. Lett.,* **29,** 1003, doi:10.029/2001GL013369.

——, ——, and J. Abshagen, 2003: A nonlinear theory for El Niño bursting. *J. Atmos. Sci.,* **60,** 152–165.

Tompkins, A., 2002: A prognostic parameterization for the subgrid scale variability of water vapor and clouds in a large-scale model and its use to diagnose cloud cover. *J. Atmos. Sci.,* **59,** 1917–1942.

Trenberth, K. E., G. W. Branstor, D. Karoly, A. Kumar, N. C. Lau, and C. Ropelewski, 1998: Progress during TOGA in understanding and modeling global teleconnections associated with tropical sea surface temperatures. *J. Geophys. Res.,* **103,** 14 291–14 324.

Wainer, I., and P. J. Webster, 1996: Monsoon/El Niño–Southern Oscillation relationships in a simple coupled ocean–atmosphere model. *J. Geophys. Res.,* **101,** 25 599–25 614.

Wallace, J. M., E. M. Rasmusson, T. P. Mitchell, V. E. Kousky, E. S. Sarachik, and H. von Storch, 1998: On the structure and evolution of ENSO-related climate variability in the tropical Pacific: Lessons from TOGA. *J. Geophys. Res.,* **103,** 14 241–14 259.

Wang, B., 1995: Interdecadal changes in El Niño onset in the last four decades. *J. Climate,* **8,** 267–285.

——, and S. I. An, 2001: Why the properties of El Niño changed during the late 1970s. *Geophys. Res. Lett.,* **28,** 3709–3712.

——, R. Wu, and X. Fu, 2000: Pacific–East Asian teleconnection: How does ENSO affect East Asian climate? *J. Climate,* **13,** 1517–1536.

Watanabe, M., and M. Kimoto, 2000: Atmosphere–ocean thermal coupling in the North Atlantic: A positive feedback. *Quart. J. Roy. Meteor. Soc.,* **126,** 3343–3369.

——, and F. F. Jin, 2003: A moist linear baroclinic model: Coupled dynamical–convective response to El Niño. *J. Climate,* **16,** 1121–1139.

Webster, P. J., 1972: Response of the tropical atmosphere to local steady flow. *Mon. Wea. Rev.,* **100,** 518–541.

——, A. M. Moore, J. P. Loschnigg, and R. R. Leben, 1999: Coupled oceanic–atmospheric dynamics in the Indian Ocean during 1997–98. *Nature,* **401,** 356–360.

Weisberg, R. H., and C. Wang, 1997: A western Pacific oscillator paradigm for the El Niño–Southern Oscillation. *Geophys. Res. Lett.,* **24,** 779–782.

Wolter, K., and M. S. Timlin, 1998: Measuring the strength of ENSO—How does 1997/98 rank? *Weather,* **53,** 315–324.

Wu, R., and B. P. Kirtman, 2003: On the impacts of the Indian summer monsoon on ENSO in a coupled GCM. *Quart. J. Roy. Meteor. Soc.,* **129,** 3439–3468.

——, and S.-P. Xie, 2003: On equatorial Pacific surface wind changes around 1977: NCEP–NCAR reanalysis versus COADS observation. *J. Climate,* **16,** 167–173.

——, and B. P. Kirtman, 2004a: Impacts of the Indian Ocean on the Indian summer monsoon–ENSO relationship. *J. Climate,* **17,** 3037–3054.

——, and ——, 2004b: Understanding the impacts of the Indian Ocean on ENSO in a coupled GCM. *J. Climate,* **17,** 4019–4031.

Xie, P., and P. Arkin, 1996: Analyses of global monthly precipitation using gauge observations, satellite estimates, and numerical model predictions. *J. Climate,* **9,** 840–858.

Xie, S.-P., H. Annamalai, F. A. Schott, and J. P. McCreary, 2002: Structure and mechanisms of south Indian Ocean climate variability. *J. Climate,* **15,** 867–878.

Yamagata, T., S. Behera, S. A. Rao, Z. Guan, K. Ashok, and N. H. Saji, 2003: Comments on "Dipoles, temperature gradients, and tropical climate anomalies." *Bull. Amer. Meteor. Soc.,* **84,** 1418–1422.

Yu, J. Y., C. R. Mechoso, J. C. McWilliams, and A. Arakawa, 2002: Impacts of Indian Ocean on ENSO cycles. *Geophys. Res. Lett.,* **29,** 1204, doi:10.1029/2001GL014098.

Yu, L. S., and M. M. Rienecker, 1999: Mechanisms for the Indian Ocean warming during the 1997–98 El Niño. *Geophys. Res. Lett.,* **26,** 735–738.

——, and ——, 2000: Indian Ocean warming of 1997–1998. *J. Geophys. Res.,* **105,** 16 923–16 939.